ACS APPLIED MATERIALS & INTERFACES

Research Article

www.acsami.org

Mesoporous TiO_2 Thin Films Exhibiting Enhanced Thermal Stability and Controllable Pore Size: Preparation and Photocatalyzed Destruction of Cationic Dyes

Jinshu Wang,* Hui Li, Hongyi Li, Chen Zou, Hong Wang, and Dasheng Li

School of Materials Science and Engineering, Beijing University of Technology, Beijing 100124, People's Republic of China

ABSTRACT: Ordered mesostructured TiO_2 thin films were constructed through a method that combined sol−gel with evaporation-induced self-assembly (EISA). It was found that the calcination temperature, as well as the type of block copolymer, could vary the TiO_2 mesoporous structure. Based on tension stress calculated by the surface energy of crystallites and the compression calculated by interface energy between the crystallites, the thermodynamic study for the sample had been carried out and the critical crystallite size expression of the mesoporous film was presented for the prediction of the thermal stability of the mesoporous structure at high temperature. It was also found that varying the mass ratio of templating agent to inorganic precursor could adjust the pore size of mesoporous TiO_2. The pore size regulating mechanism had been discussed. The sample calcined at 450−500 °C, which had a higher specific surface area and larger pore size, exhibited higher photocatalyzed destruction capability of Methylene Blue.

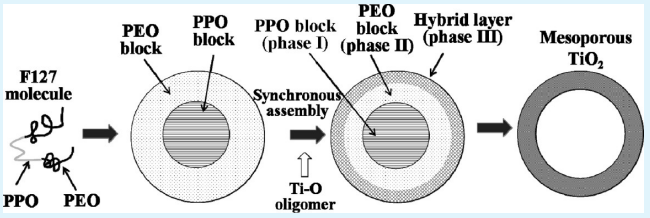

KEYWORDS: *TiO_2, mesoporous structure, film, photocatalyzed destruction*

1. INTRODUCTION

There is intense interest in the synthesis of porous solids possessing ordered pore structures with large specific surface area, because of their wide applications including catalysis, chemical and biological separation, gas sensing, molecular electronic devices, and drug delivery.[1,2] Until now, many efforts have been focused on the rational synthesis of metal oxide porous structures.[3−5] TiO_2 has aroused great attention, because of its outstanding chemical and physical properties.[6−8] The assembly of TiO_2 porous networks with well-controlled solid and pore morphologies is an active research area. Brinker et al. proposed the EISA method for the construction of well-defined TiO_2 porous materials.[9,10] However, the calcinations at temperatures over 450 °C would destroy the as-prepared mesostructure, because of the crystallization of anatase frameworks.[11,12] Currently, many efforts including chemical doping (e.g., La, Pd, SiO_2, P dopants),[13−15] templating growth[16,17] and chemical modification of precursor,[18−20] special treatment[21−23] have been carried out to improve the thermal stability of mesoporous TiO_2 framework. For example, Clement Sanchez's group reported a delayed rapid crystallization route to fabricate a TiO_2 mesostructure with highly thermal stability within a short period at 700 °C and during an extended period at 500 °C.[21,22] Zhao et al. found that carbonizing the copolymer surfactant template can be used to support TiO_2 framework during high-temperature crystallization.[23] Despite these great successes, most of these mentioned post-processing strategies are involved in some complicated procedures or introducing impurities, limiting the application of the obtained metal oxides. Recently, we have found that a thick wall was favorable for the improvement of the thermal stability, which can be formed by inhibiting the hydrolysis and condensation of the inorganic precursor and controlling the aging process of the film.[24]

Suitable titanium sources for the preparation of highly ordered mesoporous structured TiO_2 films are quite limited. Compared with inorganic sources such as TiF_4, $TiCl_4$, and $Ti(SO_4)_2$, titanium alkoxides possess important advantages in tuning the homogeneity of initial solution and in controlling final size of nanoscaled TiO_2 crystallites.[25] Typically, titanium butoxide $Ti(OBu^n)_4$ has been proved to be a good titanium source for the construction of porous TiO_2 structures.[26,27] It has a higher linearity and larger size, and the in situ released short-chain *n*-alkyl alcohol (*n*-butanol, BuOH) is very versatile to act as a co-surfactant or a swelling agent by solublizing hydrophobic additives inside the core of the micelles during the crystallization of porous TiO_2.[28−30]

In this work, we studied the effect of the types of templating agent, the concentration of block copolymer, the calcination temperature on the pore size, as well as the crystallite size of mesoporous TiO_2 prepared using $Ti(OBu^n)_4$, and we established a collapse criterion for the obtained TiO_2 mesoporous structure. It was found that the calculation results for the stability of mesostructure agreed well with the experimental results. Compared with the criterion reported in our previous work,[31] this criterion can be carried out more easily. Furthermore, the pore size regulation mechanism was investigated, and the photocatalytic activity of the as-prepared mesoporous TiO_2 materials was also studied.

Received: October 11, 2013
Accepted: December 30, 2013
Published: January 22, 2014

   dx.doi.org/10.1021/am404484k | *ACS Appl. Mater. Interfaces* 2014, 6, 1623−1631

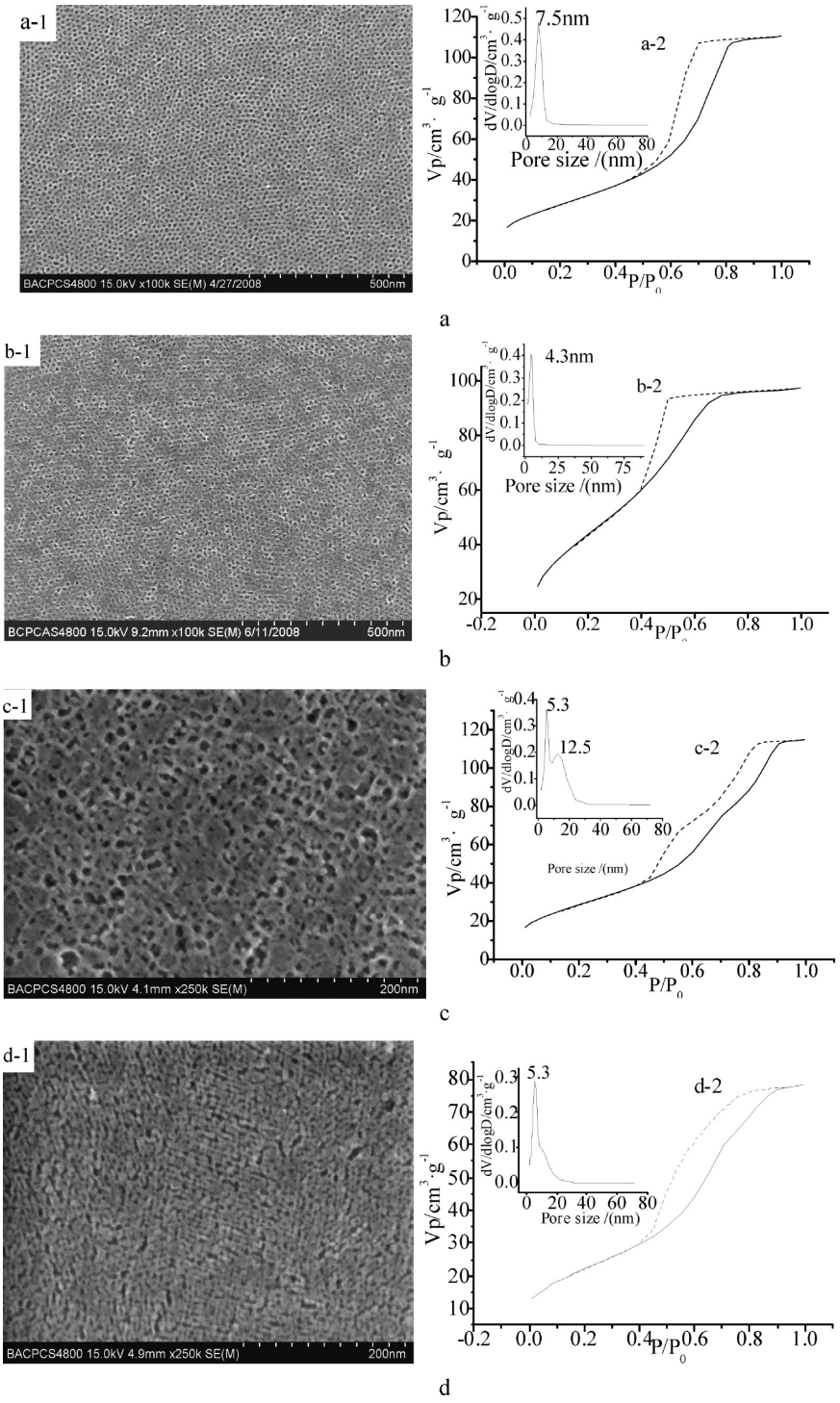

Figure 1. (Left) Scanning electron microscopy (SEM) images and (right) the corresponding N_2 adsorption−desorption isotherms and the pore size distribution curves of the TiO_2 thin fims synthesized with (a) F127, (b) F108, (c) P123, and (d) Brij58, followed by 500 °C calcinations.

2. EXPERIMENTAL SECTION

Pluronic F127 ($EO_{106}PO_{70}EO_{106}$), F108 ($EO_{133}PO_{50}EO_{133}$), P123 ($EO_{20}PO_{70}$ EO_{20}), and Brij58 ($EO_{20}CH_{16}H$) were used as the block copolymers and $Ti(OBu^n)_4$ was used as an inorganic precursor. A mixture of F127, F108, P123, and Brij58/ethanol/HCl was added dropwise to $Ti(OBu^n)_4$/ethanol/AcAc solution. The mole ratio of each component (F127, F108, P123, and Brij58/$Ti(OBu^n)_4$), relative to HCl/EtOH/AcAc, was 0.0008:0.1476, 0.0726:0.1476, 0.5036:0.1476, and 19.928:0.1476, respectively. In order to study the effect of the amount of the block copolymers on the pore size of TiO_2 mesostructure, the mass ratio of F127, relative to TBT, EtOH, and AcAc (F127:TBT:EtOH:AcAc), was designed as *X*:5g:100g:2.5g, where *X* = 0.5, 1.0, 1.5, 2.0, and 2.5g, which were assigned as S-1, S-2, S-3, S-4, and S-5, respectively. The films preparation method was similar to the TiO_2 thin films which were described in our previous paper.[31] The films were heated to different temperatures (350, 450, 500, 600, and 700 °C) and then held for 2.5 h, respectively.

3. RESULTS AND DISCUSSION

3.1. Effect of the Type of Block Copolymer on the Porous Structure of TiO_2 Films. It was reported that careful

adjustment of the precursor and polymer molecular weight (MW) could vary the TiO_2 structure.[32] Figure 1 shows the SEM micrographs together with the N_2 adsorption−desorption isotherms and the evolving pore size distribution plots of TiO_2 films prepared with different block copolymers followed by calcination at 500 °C. As shown in Figure 1a-1, the film prepared with F127 had a uniform mesoporous structure. Figure 1a-2 indicated that the sample had even cagelike pores, since the hysteresis loops were not similar to Type H1 and Type H2, but intermediate between these types; therefore, it appeared that adsorption isotherms had broad hysteresis loops and no obvious difference in the steepness of the branches of adsorption and desorption.[33] The corresponding pore size distribution results indicated that the film had narrow pore size distribution with a large pore size of 7.5 nm. On the other hand, as shown in Figure 1b, the TiO_2 film prepared with F108 also exhibited an orderly mesoporous structure (Figure 1b-1) and the samples displayed Type IV adsorption isotherms (Figure 1b-2), which are representative of the bottlelike structure. The sample had smaller pore size, compared with that prepared with F127, i.e., the pore size was only 4.3 nm. However, the samples prepared with P123 had an inhomogenous porous structure. As shown in Figure 1c, the pores in the film had irregular shape and the N_2 adsorption−desorption isotherms also indicated the irregularity. As displayed in the inset of Figure 1c-2, the film had two types of pores, with average pore sizes of 5.3 and 12.5 nm. As for the film prepared with Brji58, although some mesopores with an average pore size of 5.3 nm still existed, as shown in Figures 1d-1 and 1d-2, it was evident that the mesoporous structure deformed and collapsed. Figure 1 shows that, among these four types of block copolymer, F127 took an important role in the ordered mesostructure and bigger pores, which could be attributed to its long hydrophilic PEO and hydrophobic PPO segments, together with high molecular weight. Therefore, in the following studies, we adopted F127 as the block copolymer.

3.2. Effect of Calcination Temperature on the Structure of TiO_2 Films. Table 1 shows that the mesoporous structure could be maintained up to a temperature of 600 °C and the crystallite grew as the calcination temperature increased. The crystallite growth of anatase had been widely studied.[34,35] Praserthdam et al. studied the relationship between the TiO_2 crystallite size and the temperature, which was described as[36]

Table 1. Pore Size, Crystallite Size and Specific Surface Area of the TiO_2 Mesoporous Films Calcined at Different Temperatures[a]

T (°C)	D_p (nm)	D_e (nm)	S_{BET} ($m^2\ g^{-1}$)	D_{ec} (nm)
350	4.8	7.6	145	
450	7.8	9.0	119	
500	7.5	10.3	101	14.4
600	7.4	12.7	70	
700		29.6	19	

[a] D_p, D_e, and D_{ec} are the pore size, crystallite size, and critical crystallite size of TiO_2 mesoporous film, respectively. The sample calcined at 700 °C lost its mesoporous structure, so no pore size was provided in the table.

$$\ln \frac{d}{d_0} = k + n \ln\left(\frac{T}{\sqrt{d_0}}\right) \quad (1)$$

where d_0 is the initial TiO_2 crystallite diameter, d the TiO_2 crystallite diameter at temperature T, T the calcination temperature, n the slope of the curve, and k a constant. Taking the crystallite diameter at 350 °C as the original diameter and applying eq 1, the relationship between the crystallite diameter and the temperature was obtained, which is illustrated in Figure 2. Figure 2 demonstrates that the average crystallite size and temperature exhibited a linear relationship, as described in eq 1, in the temperature range of 450−600 °C. However, the average crystallite size of the sample calcined at 700 °C deviated from the linear segment. Kirsch studied the crystallization of mesoporous TiO_2 film, using an in situ XRD method, and found that the nucleation and growth were controlled by the surface crystallization (namely, the crystallite grew in the inside of the wall in the initial calcinations period and the growth rate decreased with further calcinations).[37]

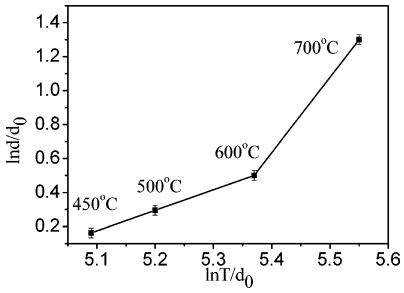

Figure 2. Relationship between ln d/d_0 and $\ln(T/d_0^{1/2})$ of the synthesized mesoporous TiO_2 samples calcined at different temperatures.

The mesostructural evolution of the synthesized TiO_2 thin films with temperature is shown in Figure 3. As shown in Figure 3, ordered mesoporous structure was found for the TiO_2 films except for the sample prepared by calcination at 700 °C. When the sample was calcined at 350 °C, as shown in Figure 3a, many organic compounds still remained on the surface of the films, as a result of parts of pores being blocked. When the calcination temperature was increased to 500 °C, as shown in Figure 3b, a uniform and ordered mesoporous structure was clearly shown in the sample without any substance absorbed on the film surface. Increasing the temperature to 600 °C, a uniformly ordered mesoporous structure was still maintained without the collapse of the mesoporous structure (Figure 3c). In order to investigate the mesoporous structure clearly, TEM observation was carried out for the films. As shown in Figure 3e, the sample calcined at 600 °C had a well-organized mesostructure, with a wall thickness of ∼10−13 nm. Further increasing the temperature to 700 °C, the sample lost its initial mesostructure and wormlike particles existed in the film, because of overgrowth of the grains, as shown in Figures 3d and 3f. From Figure 3e, we could deduce that the thick wall of the framework played an important role in the highly thermal stability of the sample, as shown by its mesoporous structure being manitained at 600 °C at least for 2.5 h.

Further analysis of the microstructure of the synthesized thin films has been carried out through the cross-sectional TEM images of the film calcined at 500 °C, as shown in Figure 4. The testing sample was prepared by the copper-coated method. As

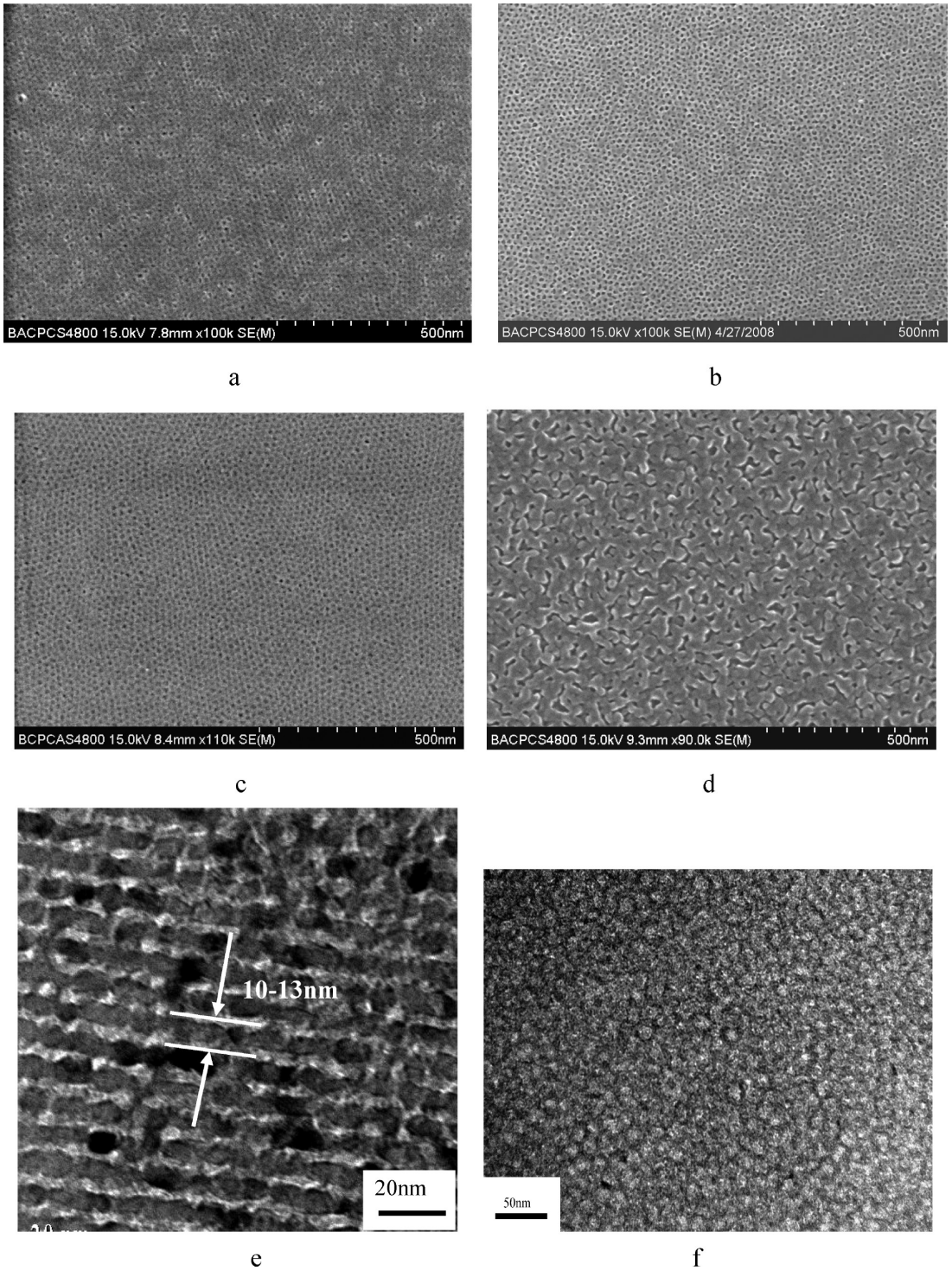

Figure 3. (a–d) SEM images of the synthesized mesoporous TiO_2 thin films (calcined at (a) 350, (b) 500, (c) 600, and (d) 700 °C) and (e,f) TEM images of the synthesized mesoporous TiO_2 thin films (calcined at (e) 600 and (f) 700 °C).

indicated by the TEM image in Figure 4a, the thickness of the calcined mesoporous TiO_2 thin film was ~220 nm. No obvious boundaries between the layers were found. More-detailed structural information could be obtained by HRTEM images (Figures 4b and 4c). The honeycomb structure of the framework could be clearly observed throughout the thickness of the film (Figure 4b). Unlike the well-aligned mesostructure of the top view, the mesopores (white area) distributed randomly in the framework. The entire wall structure displayed an anatase lattice fringe, indicating the highly crystalline nature of the film. The anatase crystallites that were embedded in the framework (see Figure 4c) were oriented randomly, which allowed the crystallites to nucleate and grow within the limited space of the pore wall, avoiding destruction of the mesostructure. The fast Fourier transform (FFT) of the image (inset, Figure 4c) indicated the presence of 4-fold symmetry.[38]

dx.doi.org/10.1021/am404484k | ACS Appl. Mater. Interfaces 2014, 6, 1623–1631

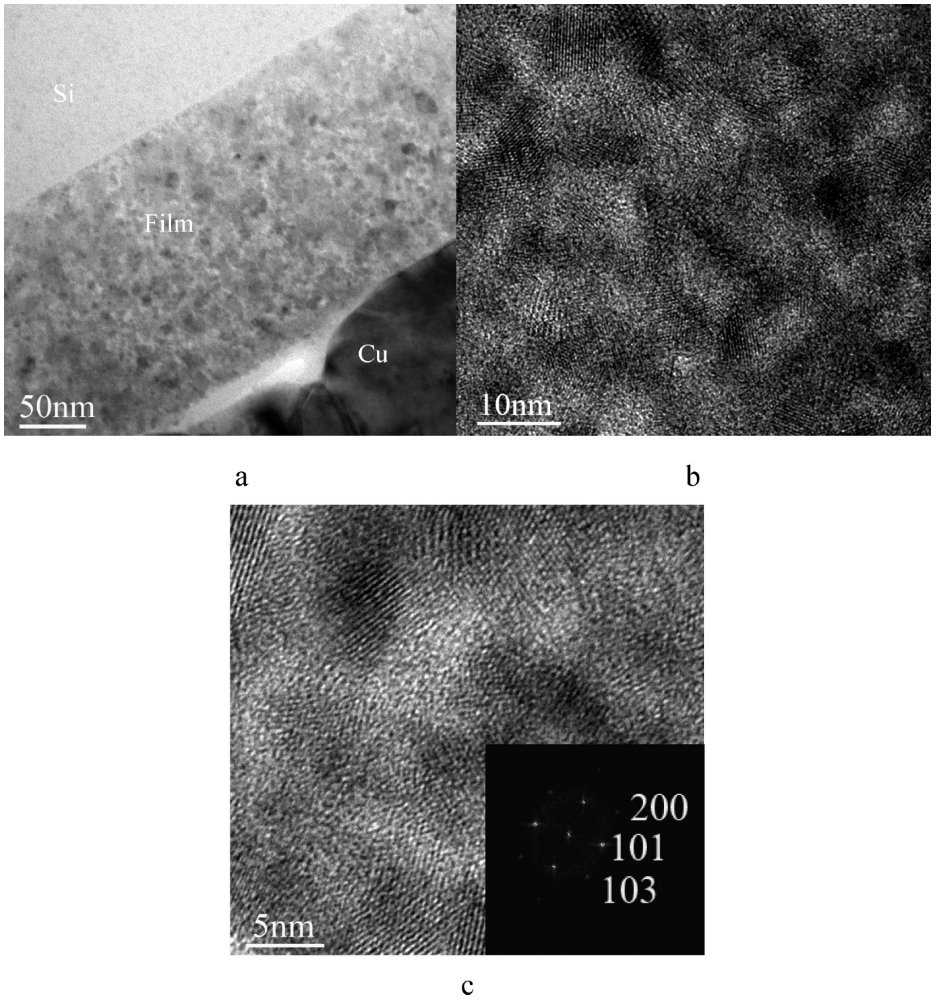

Figure 4. Cross-sectional TEM images of the as-made mesostructured TiO_2 film calcined at 500 °C with different magnifications ((a) TEM iamge and (b, c) HRTEM images). Inset in panel (c) is the corresponding two-dimensional fast Fourier transformation (FFT) patterns of the full image.

The Barrett–Joyner–Halenda (BJH) pore size analysis (Figure 5) performed on the adsorption branches indicated that the samples calcined at <600 °C had a narrow pore size distribution. The structural parameters of the films at different calcination temperatures are listed in Table 1. The sample calcined at 350 °C possessed a small mean pore size of 4.8 nm, whereas the sample calcined at 450 °C was 7.8 nm. Furthermore, although the calcination temperatures increased from 450 °C to 500 °C and then 600 °C, not much difference was observed for the pore diameter, indicating the high thermal stability of the films. The BET specific surface area was lower than those reported for mesoporous TiO_2 materials synthesized by templating F127.[39,40] This might be attributed to the thick inorganic walls of our samples. From the adsorption isotherms measured at 700 °C, it could be seen that the sample had a broad pore size distribution due to the collapse of most pore walls, which was consistent with the SEM and TEM observations in Figures 3d and 3f, respectively.

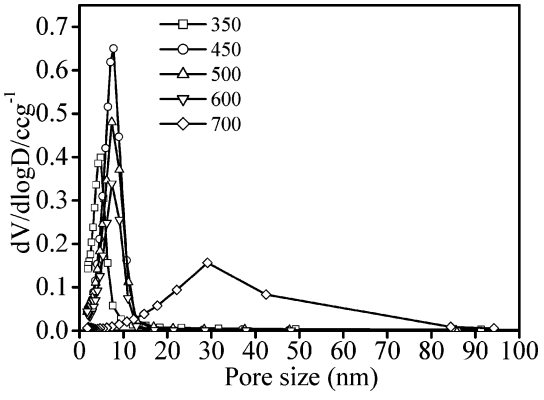

Figure 5. Pore size distribution curves for the synthesized samples calcined at 350, 450, 500, 600, and 700 °C.

Raman method was carried out for the analysis of crystallites, since it was more suitable for the nanosized particle. The Raman spectra of TiO_2 films prepared at different temperatures is shown in Figure 6. The wave shift at 146, 199, 398, 517 and 641 cm^{-1} were caused by the vibration of anatase,[41,42] in which the wave shifts at 146, 199, and 641 cm^{-1} could be attributed to the Eg vibration model and those at 398 and 517 cm^{-1} were designed as the B1g model.

As shown in Figure 6, five obvious Raman peaks existed in the five samples. The Raman vibration spectra displayed that anatase nanparticles had been obtained in the sample calcined at 350 °C. The Raman vibration frequency of the nanosized TiO_2 was different from the ordinary TiO_2, i.e., the lowest frequencies E_g of mesoporous TiO_2 calcined at 350 and 700 °C were 145 and 177 cm^{-1}, respectively, indicating that the Raman

dx.doi.org/10.1021/am404484k | ACS Appl. Mater. Interfaces 2014, 6, 1623–1631

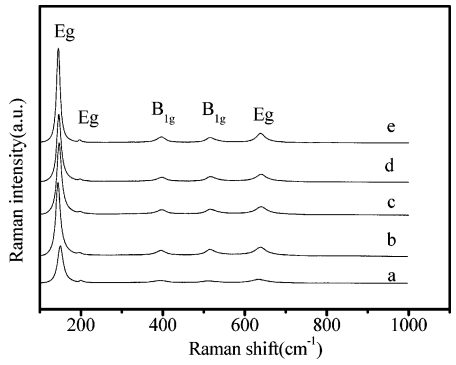

Figure 6. Raman patterns of prepared mesoporous samples calcined at 350 °C (pattern a), 450 °C (pattern b), 500 °C (pattern c), 600 °C (pattern d), and 700 °C (pattern e).

peak moved to the higher frequency side, which might be caused by the following two reasons: one was caused by the nanosized particles due to the blue shift of Raman frequency, and the another was caused by the oxygen vacancies.[43] As for our sample that was calcined in oxygen, the oxygen vacancies in the samples might be neglected; therefore, the blue shift of Raman frequency might be caused by the smaller crystallite size. The crystallite size increased as the calcination temperature increased. Raman results also indicated that the TiO_2 appeared to be anatase, even under high temperature (700 °C). Retardation of the anatase−rutile transformation was probably due to the presence of acetyl acetone, which can make anatase stable up to 800 °C.[44]

3.3. Thermal Stability of Mesoporus TiO_2 Film. The thermal stability of the film is correlated with the temperature. The prediction of the mesoporous structure at different temperatures is important. A four-coordinate channel mode was proposed, and the equation based on thermodynamic calculation has been established.[31]

$$J = \frac{4D_{\mathrm{eff}}}{kT(D_{\mathrm{p}} + 0.87D_{\mathrm{e}})}\left[\gamma_{\mathrm{interf}}\frac{(-D_{\mathrm{p}} + \sqrt{0.90D_{\mathrm{e}}^2 - D_{\mathrm{p}}^2})}{\pi D_{\mathrm{p}}} - \gamma_{\mathrm{surf}}\right] \quad (2)$$

where D_p is the size of mesopores, D_e is the size of crystallites, D_{eff} is the effective coefficient, and γ_{interf} and γ_{surf} are the interface energy and surface energy, respectively. T is the temperature.

In the previous work, we presented that the mesoporous structure stability could be predicted by the value of J. When $J > 0$, the particles would diffuse toward the pores, causing the collapse of the mesoporous structure. Otherwise, the mesoporous structure would be stable. However, this method is relatively complicated, since the value of J must be calculated based on the measured data. Therefore, in this work, we deduced another method to predict the thermal stability of the mesoporous structure.

From the discussion above, it could be found that the critical condition for the thermally stable mesoporous structure could be obtained at $J = 0$. Therefore, the critical crystallite size (D_{ec}) could be calculated and expressed as

$$D_{\mathrm{ec}} = \sqrt{\frac{\left[\left(\frac{\gamma_{\mathrm{surf}}}{\gamma_{\mathrm{interf}}}\right)D_{\mathrm{p}} + \frac{1}{\pi}\right]^2 + D_{\mathrm{p}}^2}{0.90}} \quad (3)$$

The surface energy and interface energy of TiO_2 could be calculated based on eqs 4 and 5, respectively:[45]

$$\gamma_{\mathrm{surf}} = 1.91 - 1.48 \times 10^{-4}(T - 298) \quad (4)$$

$$\gamma_{\mathrm{interf}} = 1.32 - 1.48 \times 10^{-4}(T - 298) \quad (5)$$

The TiO_2 critical crystallite size (D_{ec}) of the mesoporous film could be calculated based on eqs 3−5 and is shown in eq 6:

$$D_{\mathrm{ec}} = \sqrt{\frac{\left\{\left[\frac{1.91 - 1.48 \times 10^{-4}(T-298)}{1.32 - 1.48 \times 10^{-4}(T-298)}D_{\mathrm{p}}\right] + \frac{1}{\pi}\right\}^2 + D_{\mathrm{p}}^2}{0.90}}$$

$$\approx \sqrt{\frac{(1.45D_{\mathrm{p}} + 0.32)^2 + D_{\mathrm{p}}^2}{0.90}} \quad (6)$$

When $D_e > D_{ec}$, the crystallites exceeded the critical crystallite size and the substance diffused into the mesopores, leading to the collapse of the mesoporus structure. When $D_e < D_{ec}$, the TiO_2 film kept its mesoporous structure.

As shown in Table 1, the mesoporous film had the pore size in the range of 7.4−7.8 nm in the temperature range of 450−600 °C. Supposing that the average pore diameter of the film is 7.6 nm (the mean value between 7.4 nm and 7.8 nm), based on eq 6, the critical crystallite size D_{ec} of the TiO_2 mesoporous film could be calculated as 14.4 nm. The crystallite size (D_e) of the films calcined at temperatures of <600 °C was smaller than D_{ec}, indicating that the films kept their mesoporous structure. For the film calcined at 700 °C, D_e = 29.6 nm, which is larger than the critical value; therefore, the mesoporous structure collapsed. The above results indicate that the experimental results were consistent with the calculation results for the prediction of the thermal stability.

3.4. Regulation of Pore Size. The XRD patterns of mesoporous TiO_2 samples synthesized using F127 as the templating agent and $Ti(OBu^n)_4$ as the precursor with different mass ratios followed by calcinations at 500 °C are shown in Figure 7. The small-angle XRD results indicated that the thin

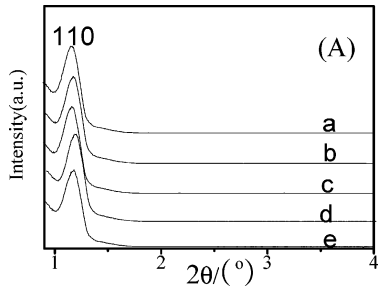

Figure 7. Small-angle XRD patterns of the synthesized thin films. (a) S-1, (b) S-2, (c) S-3, (d) S-4, and (e) S-5.

films had highly organized mesoporous framework. Table 2 shows the pore size and crystallite size of the mesoporous film prepared with different mass ratios. As presented in Table 2, the crystallite size decreased and the pore size increased with the increase of mass ratio of F127/$Ti(OBu^n)_4$, i.e., when the F127/$Ti(OBu^n)_4$ mass ratio increased from 0.1 to 0.5, the crystallite size decreased from 14.3 nm to 8.9 nm and the pore size increased from 5.4 nm to 9.1 nm, respectively, indicating that the wall thickness decreased.

dx.doi.org/10.1021/am404484k | ACS Appl. Mater. Interfaces 2014, 6, 1623−1631

Table 2. Textural Parameters of the Synthesized Mesoporous TiO_2 Materials Prepared with Different Mass Ratios of F127/$Ti(OBu^n)_4$

sample	F127/$Ti(OBu^n)_4$ mass ratio	D_p[a] (nm)	D[b] (nm)
S-1	0.1	5.4	14.3
S-2	0.2	6.2	13.6
S-3	0.3	7.1	11.2
S-4	0.4	7.4	10.2
S-5	0.5	9.1	8.9

[a]BJH average pore size. [b]Average crystallite size.

The above results show that the pore size of the samples could be regulated by the mass ratio of F127/$Ti(OBu^n)_4$. The pore size regulation mechanism could be explained as follows. Taking triblock-copolymer Pluronic F127 as the templating agent was the premise for the formation of the mesoporous TiO_2 with different pore size. F127 is a unique surfactant, because of its high molecular weight with long hydrophilic PEO and hydrophobic PPO blocks, which offers the possibilities of the formation of hydrophobic core (PPO) of the micelles and hydrophilic corona with a certain thickness. According to the "three-phase model", which was presented for a silica mesoporous structure,[43] Ti-oxo species might react with micelles to form a three-phase structure. Figure 8 shows the schematic diagram of the formation of the synthesized mesoporous TiO_2 materials with different pore size. As shown in Figure 8, hydrophobic phase I (PPO) was located in the center, and the PEO chains II existed in two parts, namely, embedding in the Ti-oxo matrix and situating between the hydrophobic core (phase I) and the Ti-oxo (this part of PEO is called as phase II). In other words, a part of the PEO chains might form a separate "phase" between the hydrophobic block and the Ti-oxo species. This part of the PEO also contributed to the mesoporosity. In other words, since the templating agent could form micelles with a fixed thickness of the PEO under certain conditions, the change of the organic–inorganic hybrid material (phase III) would change the thickness of the rest of the PEO (phase II). Therefore, the thickness of the organic–inorganic hybrid material could be changed by adjusting the mass ratio of templating agent to inorganic precursor, resulting in the change of pore size. It is known that the pore size is, to a large extent, dependent on the effective volume of the hydrophobic core (PPO) of the micelles. As shown in Table 2, when the concentration of templating agent F127 was low, a greater number of oligomeric Ti-oxo species could assembly with PEO chains to form an inorganic–organic hybrid (phase III); therefore, only a small number of PEO chains (phase II) contributed to the microporosity with the result of small pores in the framework. Since the concentration of precursor was fixed, the number of Ti-oxo species that could assemble with ethylene oxide decreased as the concentration of F127 increased. Therefore, a greater number of PEO chains would contribute to the microposity, resulting in the formation of large pores and the decrease of the wall thickness of mesoporous TiO_2. Since the pore size of the mesoporous network was primarily dependent on the hydrophobic core diameter, the *n*-butanol released by $Ti(OBu^n)_4$ was inclined to penetrate the interface between the hydrophilic and hydrophobic domains of micelles, and located at the hydrophobic core due to the nonpolar nature; therefore, *n*-butanol in situ also played a pronounced role in the construction of a large-pore mesostructured TiO_2 framework.

3.5. Photocatalytic Activity. The photocatalytic activity was evaluated by photodegradation of Methylene Blue, and the detailed measurement method has been described in our previous paper.[46] Figure 9 shows the illumination time dependence of photodegradation property of Methylene Blue, using different mesoporous TiO_2 under an irradiating high-pressure mercury arc. It was clear that the sample calcined at 350 °C exhibited low photocatalytic activity, because of its amorphous phase, and remained composed of organic compounds. Apart from the low crystallinity, the defects in the sample might become the recombination center of photogenerated holes and electrons, resulting in worse photocatalytic activity of the semiconductor. Only 29% MB was degraded after light irradiation for 180 min. Increasing the calcination temperature resulted in great improvement in the photocatalytic activity. Samples calcined at 450 and 500 °C

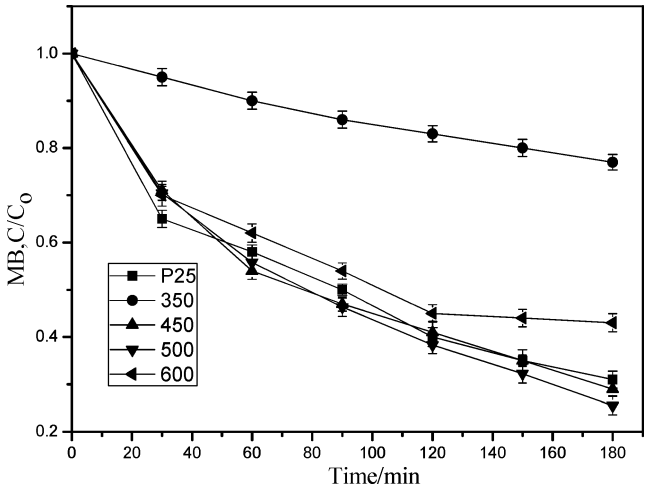

Figure 9. Photocatalyzed destruction of Methylene Blue of different samples.

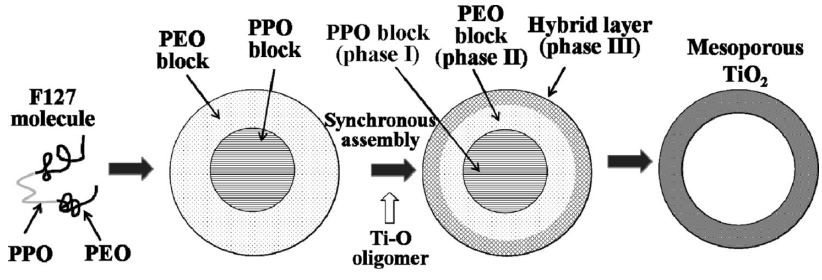

Figure 8. Schematic diagram of the formation of the synthesized mesoporous TiO_2 materials with different pore size.

photodegraded more than 70% MB (75% for the sample calcined at 500 °C, 71% for that calcined at 450 °C) in the same duration, which were superior to that of P25 (69% MB was photodegraded). However, the sample calcined at 600 °C showed relatively poor photocatalytic activity. 55% MB was photodegraded after being irradiated for 120 min and kept almost stable with an irradiation time up to 180 min. As shown in Table 1, the samples calcined at 450 and 500 °C had smaller crystallite size, higher specific surface area, and larger pore size and porosity. It is well-known that the larger specific surface area results in higher adsorption ability of MB. In addition, photogenerated carriers inside the nanoparticles are easier to diffuse to their surface, decreasing the recombination ratio of photogenerated electrons and holes. Furthermore, the high porosity can increase adsorption capability of the organic pollutant and the amount of hydroxyl radicals. Consequently, the mesoporous TiO_2 calcined at 500 °C had higher photocatalyzed destruction capability of MB, because of its larger specific surface area and mesopore volume. Increasing temperature to 600 °C, the photocatalytic activity decreased due to the growth of the crystallites and decrease of the specific surface area. In addition, it was also notable that the mesoporous TiO_2 calcined at 450 and 500 °C exhibited greater photocatalytic capability than P-25 in the ultraviolet light range.

4. CONCLUSIONS

In summary, TiO_2 mesoporous films had been obtained using the $Ti(OBu^n)_4$–EtOH–HCl system with different templating agents through sol–gel and EISA methods. It was found that, among F127, F108, P123, and Brij58, using F127 as the templating agent was easy for preparing mesoporous TiO_2 that exhibited an excellent thermal stability. The TiO_2 film could keep the mesoporous structure up to 600 °C, but the structure would collapse with further increases in the calcination temperature. The thermal stability of the TiO_2 mesoporous film could be predicated using the thermodynamic method, and mesoporous structure collapse criterion was obtained as

$$D_{ec} = \sqrt{\frac{(1.45D_p + 0.32)^2 + D_p^2}{0.90}}$$

where D_p and D_{ec} were the sizes of mesopores and critical crystallites, respectively.

When crystallite size D_e at a certain temperature was smaller than D_{ec}, the mesoporous structure remained stable; otherwise, the mesoporous structure would collapse. This criterion could be applied to determine the thermal stability of the available TiO_2 films with provided mesopore size and crystallite size at a certain temperature. Furthermore, eq 3 could be a universal one for predicting the thermal stability of mesoporous films composed of other substances. The pore size could be adjusted by varying the mass ratio of templating agent to inorganic precursor. The mesoporous TiO_2 calcined at proper temperature, which had higher specific surface area and smaller crystallite size, had a higher capability of photocatalyzed destruction of Methylene Blue.

AUTHOR INFORMATION

Corresponding Author

*E-mail: wangjsh@bjut.edu.cn.

Notes

The authors declare no competing financial interest.

ACKNOWLEDGMENTS

This work was supported by National Outstanding Young Investigator Grant of China (No. 51225402), National Natural Science Foundation of China (NSFC) (Nos. 51071005 and 51002004), Beijing Municipal Commission of Education Foundation (Nos. KZ201010005001 and KM201110005003), Beijing Innovation Talent Project.

REFERENCES

(1) Soler-Illia, G. J. D. A. A.; Sanchez, C.; Lebeau, B.; Patarin, J. *Chem. Rev.* **2002**, *102*, 4093–4138.
(2) Goethals, E. C.; Elbaz, A.; Lopata, A. L.; Bhargava, S. K.; Bansal, V. *Langmuir* **2013**, *29* (2), 658–666.
(3) Lin, X.; Rong, F.; Ji, X.; Fu, D. *Microporous Mesoporous Mater.* **2011**, *142*, 276–281.
(4) Pan, J.; Zhao, X. S.; Lee, W. I. *Chem. Eng. J.* **2010**, *2-3*, 363–380.
(5) Crepaldi, E. L.; Soler-Illia, G. D. A. A.; Bouchara, A.; Grosso, D.; Durand, D.; Sanchez, C. *Angew. Chem., Int. Ed.* **2003**, *42*, 347–351.
(6) Leshuk, T.; Parviz, R.; Everett, P.; Krishnakumar, H.; Varin, R. A.; Gu, F. *ACS Appl. Mater. Interfaces* **2013**, *5* (6), 1892–1895.
(7) Natoli, A.; Cabeza, A.; De la Torre, A. G.; Aranda, M. A. G.; Santacruz, I. *J. Am. Ceram. Soc.* **2012**, *95*, 502–508.
(8) Pan, X.; Zhao, Y.; Liu, S.; Korzeniewski, C. L.; Wang, S.; Fan, Z. *ACS Appl. Mater. Interfaces* **2012**, *4* (8), 3944–3950.
(9) Brinker, C.J.; Lu, Y.; Sellinger, A.; Fan, H. *Adv. Mater.* **1999**, *11*, 579–585.
(10) Lu, Y.; Ganguli, R.; Drewien, C. A.; Anderson, M. T.; Brinker, C. J.; Gong, W.; Guo, Y.; Soyez, H.; Dunn, B.; Huang, M. H.; Zink, J. I. *Nature* **1997**, *389*, 364–368.
(11) Lei, C.X.; Zhou, H.; Wang, C.; Feng, Z. *Electrochim. Acta* **2013**, *87* (1), 245–249.
(12) Hongo, T.; Yamazaki, A. *Microporous Mesoporous Mater.* **2011**, *142*, 316–321.
(13) Yuan, S.; Sheng, Q. R.; Zhang, J. L.; Yamashita, H.; He, D. N. *Microporous Mesoporous Mater.* **2008**, *110*, 501–507.
(14) He, C. X.; Tian, B. Z.; Zhang, J. L. *J. Colloid Interface Sci.* **2010**, *344*, 382–389.
(15) Yu, H. F. *J. Phys. Chem. Solids* **2007**, *68*, 600–607.
(16) Zakaria, M. B.; Suzuki, N.; Torad, N. L.; Matsuura, M.; Maekawa, K.; Tanabe, H.; Yamauchi, Y. *Eur. J. Inorg. Chem.* **2013**, 2330–2335.
(17) Ortel, E.; Fischer, A.; Chuenchom, L.; Polte, J.; Emmerling, F.; Smarsly, B.; Kraehnert, R. *Small* **2012**, *8*, 298–309.
(18) Khimich, N. N.; Venzel, B. I.; Drozdova, I. A.; Koptelova, L. A. *Russ. J. Appl. Chem.* **2002**, *75*, 1108–1112.
(19) Lackhoff, M.; Prieto, X.; Nestle, N.; Dehn, F.; Niessner, R. *Appl. Catal., B* **2003**, *43*, 205–216.
(20) Etacheri, V.; Seery, M. K.; Hinder, S. J.; Pillai, S. C. *Adv. Funct. Mater.* **2011**, *21*, 3744–3752.
(21) Grosso, D.; Soler-Illia, G. J. A. A.; Crepaldi, E.o. L.; Cagnol, F.; Sinturel, C.; Bourgeois, A.; Bruneau, A. B.; Amenitsch, H.; Albouy, P. A.; Sanchez, C. *Chem. Mater.* **2003**, *15*, 4562–4570.
(22) Ferrero, E. M.; Grosso, D.; Boissiere, C.; Sanchez, C.; Oms, O.; Leclercq, D.; Vioux, A.; Miomandrec, F.; Audebert, P. *J. Mater. Chem.* **2006**, *16*, 3762–3767.
(23) Zhang, R. Y.; Tu, B.; Zhao, D. Y. *Chem.—Eur. J.* **2010**, *16*, 9977–9981.
(24) Li, H.; Wang, J. S.; Li, H. Y.; Yin, S.; Sato, T. *Mater. Lett.* **2009**, *63*, 1583–1585.
(25) Pan, J. H.; Zhang, X.; Du, A. J.; Sun, D. D.; Leckie, J. O. *J. Am. Chem. Soc.* **2008**, *130*, 11256–11257.
(26) Calleja, G.; Serrano, D. P.; Sanz, R.; Pizarro, P.; Garcia, A. *Ind. Eng. Chem. Res.* **2004**, *43*, 2485–2492.
(27) Liu, K. S.; Fu, H. G.; Shi, K. Y.; Xin, B. F; Jing, L. Q.; Zhou, W. *Nanotechnology* **2006**, *17* (15), 3641–3648.
(28) Feng, P.; Bu, X.; Pine, D. J. *Langmuir* **2000**, *16*, 5304–5310.
(29) Kleitz, F.; Blanchard, J.; Zibrowius, B.; Schüth, F.; Ågren, P.; Lindén, I. M. *Langmuir* **2002**, *18*, 4963–4971.

(30) Kleitz, F.; Blanchard, J.; Zibrowius, B.; Schüth, F.; Ågren, P.; Lindén, I. M. *Langmuir* **2002**, *18*, 4963−4971.
(31) Wang, J. S.; Li, H.; Li, H. Y.; Zou, C. *J. Phys. Chem. C* **2012**, *116* (17), 9517−9525.
(32) Kim, D. J.; Kim, S. J.; Roh, D. K.; Kim, J. H. *Phys. Chem. Chem. Phys.* **2013**, *15*, 7345−7353.
(33) Kruk, M.; Jaroniec, M. *Chem. Mater.* **2001**, *13* (10), 3169−3183.
(34) Fattakhova-Rohlfing, D.; Wark, M.; Brezesinski, T.; Smarsly, B. M.; Rathouský, J. *Adv. Funct. Mater.* **2007**, *17*, 123−132.
(35) Coakley, K. M.; Liu, Y. X.; McGehee, M. D.; Frindell, K. L.; Stucky, G. D. *Adv. Funct. Mater.* **2003**, *13* (4), 301−306.
(36) Praserthdam, P.; Silveston, P. L.; Mekasuwandumrong, O.; Pavarajarn, V.; Phungphadung, J.; Somrang, P. *Cryst. Growth Des.* **2004**, *4* (1), 39−43.
(37) Kirsch, B. L.; Richman, E. K.; Riley, A. E.; Tolbert, S. H. *J. Phys. Chem. B* **2004**, *108* (34), 12698−12706.
(38) Yoo, S.; Ford, D. M.; Shantz, D. F. *Langmuir* **2006**, *22*, 1839−1845.
(39) Crepaldi, E. L.; Soler-Illia, G. J. d. A. A.; Grosso, D.; Sanchez, C. *New J. Chem.* **2003**, *27*, 9−13.
(40) Lancelle-Beltran, E.; Prené, P.; Boscher, C.; Belleville, P.; Buvat, P.; Lambert, S.; Guillet, F.; Boissière, C.; Grosso, D.; Sanchez, C. *Chem. Mater.* **2006**, *18*, 6152−6156.
(41) Zhang, W. F.; He, Y. L.; Zhang, M. S.; Yin, Z.; Chen, Q. *J. Phys. D: Appl. Phys* **2000**, *33*, 912−916.
(42) Parker, J. C.; Siegel, R. W. *Appl. Phys. Lett.* **1990**, *57* (9), 943−945.
(43) Smarsly, B.; Polarz, S.; Antonietti, M. *J. Phys. Chem. B* **2001**, *105* (43), 10473−10483.
(44) Djaoued, Y. *J. Sol−Gel Sci. Technol.* **2002**, *24*, 255−264.
(45) Yin, L.; Zhou, Q. F. *Funct. Mater.* **2000**, *2*, 186−189.
(46) Wang, J. S.; Li, H.; Li, H. Y.; Zou, C.; Zhou, M. L. *Solid State Sci.* **2010**, *4*, 490−497.